
InterNet: Unsupervised Cross-modal Homography Estimation Based on Interleaved Modality Transfer and Self-supervised Homography Prediction

Junchen Yu¹ Si-Yuan Cao^{1,2*} Runmin Zhang¹ Chenghao Zhang¹
Jianxin Hu¹ Zhu Yu¹ Beinan Yu^{1,3} Hui-Liang Shen¹

¹College of Information Science and Electronic Engineering, Zhejiang University
²Ningbo Innovation Center, Zhejiang University ³Jinhua Institute, Zhejiang University

Abstract

We propose a novel unsupervised cross-modal homography estimation framework, based on interleaved modality transfer and self-supervised homography prediction, named InterNet. InterNet integrates modality transfer and self-supervised homography estimation, introducing an innovative interleaved optimization framework to alternately promote both components. The modality transfer gradually narrows the modality gaps, facilitating the self-supervised homography estimation to fully leverage the synthetic intra-modal data. The self-supervised homography estimation progressively achieves reliable predictions, thereby providing robust cross-modal supervision for the modality transfer. To further boost the estimation accuracy, we also formulate a fine-grained homography feature loss to improve the connection between two components. Furthermore, we employ a simple yet effective distillation training technique to reduce model parameters and improve cross-domain generalization ability while maintaining comparable performance. Experiments reveal that InterNet achieves the state-of-the-art (SOTA) performance among unsupervised methods, and even outperforms many supervised methods such as MHN and LocalTrans. Source code is available at <https://github.com/Junchen-Yu/InterNet>.

1 Introduction

Cross-modal homography estimation aims to solve the global perspective transformation between two images under different modalities. It is widely used in various computer vision tasks, such as GPS-denied robotic localization [1, 2], multi-modal image restoration [3, 4], and multi-spectral image fusion [5, 6]. Recent supervised homography estimation approaches [7–12] have demonstrated their superiority in handling large modality gaps and deformations. However, since the multi-modal images are captured through different imaging sensors, the ground-truth homography deformations are usually unknown in real-world applications.

To avoid using labeled data, unsupervised homography estimation methods have emerged. Existing approaches typically optimize the similarity between the warped source image and target image through intensity-based losses. Nguyen *et al.* [13] adopted a pixel-wise photometric loss as the similarity metric. Following this pioneer research, the works [14–16] projected input images into consistent deep features for both homography estimation and supervision, improving the robustness under illumination changes. To deal with large deformations, Koguchiuk *et al.* [17] replaced the photometric loss with a perceptual loss. Besides, some multi-modal image registration approaches [18, 19] transferred an image into another modality, allowing the use of mono-modality similarity metrics for network training. However, the above approaches mainly indirectly learned the matching process through intensity-based similarity metrics, which lack the direct knowledge injection of homography transformation. Moreover, most of these approaches [14–16, 18] coupled the training process of

*Corresponding author.

image registration with consistent feature extraction or modality transfer, making the network hard to optimize when the deformation or modality gap grows. According to our experiments, these designs lead to difficulties in network convergence, especially when applying the current state-of-the-art (SOTA) iterative architectures [11, 12] for homography estimation.

To address the above problem, in this paper, we propose an interleaved modality transfer and self-supervised homography prediction network, named InterNet, for unsupervised cross-modal homography estimation. Inspired by the alternating direction method of multipliers (ADMM) and the split Bregman method, we introduce an interleaved optimization framework to alternately train the modality transfer and homography estimation modules. In this manner, the original complex optimization problem is decoupled into more manageable sub-problems, ensuring better convergence properties. Better still, after modality transfer, the inputs to the homography estimation module can approximately be considered as mono-modality. This enables the use of synthetic intra-modal data with ground-truth homographies to provide the direct knowledge of homography transformation in a self-supervised manner. Through the interleaved training strategy, the modality transfer module gradually narrows the modality gap and provides more suitable inputs for the homography estimation module, while the homography estimation module provides more accurate estimation results and offers more reliable supervision for the modality transfer module. To further strengthen the mutual promotion of two modules, we formulate a fine-grained homography feature (FGHomo) loss to constrain the feature consistency in the homography estimation module. Finally, we introduce a simple yet effective distillation training technique, which significantly reduces model parameters and improves cross-domain generalization ability, despite causing a slight performance drop.

We evaluate our InterNet on a variety of datasets including GoogleMap [10], DPDN [20], WHU-OPT-SAR [21], and Flash/no-flash [22] cross-modal datasets, RGB/NIR [23] cross-spectral datasets, and PDS-COCO [17] photometrically distorted datasets. Our InterNet outperforms all unsupervised homography estimation approaches with a large gap, while even achieving better performance than many supervised approaches. We note that InterNet owns 54.3% and 47.4% lower mean average corner errors (MACEs) than MHN [8], and 61.8% and 85.8% lower MACEs than LocalTrans [9] on the challenging GoogleMap and WHU-OPT-SAR datasets, respectively. To summarize, our main contributions are as follows:

- We propose a novel unsupervised cross-modal homography estimation framework, named InterNet. InterNet can be trained without any labeled data, while handling the homography estimation under large modality gaps and deformations. Experimental results reveal that our InterNet achieves SOTA performance among unsupervised methods, and even outperforms many supervised methods such as MHN [8] and LocalTrans [9].
- We design an interleaved unsupervised training framework that uses modality transfer and self-supervised homography prediction, involving an interleaved optimization process that cyclically narrows modality gaps and improves cross-modal homography estimation performance. Furthermore, we adopt a simple yet effective distillation training technique to reduce model parameters and improve cross-domain generalization with little impact on performance.
- To further boost the optimization effectiveness of the interleaved framework, we introduce a fine-grained homography feature loss that promotes feature consistency in the homography estimation module after the modality transfer. This enhances mutual interactions between two modules and improves overall performance.

2 Related Works

Traditional Homography Estimation. Traditional homography estimation approaches are broadly classified into two categories: feature-based and direct approaches. Direct approaches estimate homography from pixel intensities. The classic Lucas-Kanade (LK) algorithm [24, 25] iteratively estimates the residual homography using a pre-computed iterator. As for feature-based approaches, homography estimation involves the extraction of feature descriptors, such as SIFT [26], SURF [27], ORB [28], LIFT [29] and LoFTR [30]. Robust estimation techniques like RANSAC [31], MAGSAC [32], and IRLS [33] are then applied for outlier rejection during homography estimation.

Supervised Deep Homography Estimation. DeTone *et al.* [7] first introduced the seminal DHN, a VGG-style network to predict the homography using the concatenated source and target images. Many

subsequent works have been presented to further enhance the accuracy of homography estimation. MHN [8] introduced a multiscale VGG-style network to iteratively predict the residual homography. CLKN [34] combined CNN with an untrainable IC-LK iterator for recurrent homography estimation. DLKFM [10] enhanced the similarity of the feature maps with a new loss function to improve the performance of IC-LK iterator. LocalTrans [9] adopted a multiscale transformer with local attention to progressively register cross-resolution images. IHN [11] substantially improved the estimation accuracy through a designed trainable iterative framework. RHWF [12] further introduced homography-guided image warping and focus transformer into the recurrent framework, achieving higher accuracy.

Unsupervised Deep Homography Estimation. Nguyen *et al.* [13] proposed an unsupervised homography estimation network that trained with pixel-level photometric loss. Following this work, Zhang *et al.* [14] introduced CA-UDHN, which projects the input images into consistent feature space for effective estimation. Koguchiuk *et al.* [17] expanded CA-UDHN, replacing the photometric loss with perceptual loss [35] to enhance the robustness of unsupervised homography estimation against variations in intensity and viewpoint. Ye *et al.* [15] enforced the image feature to be warp-equivalent with a feature identity loss and proposed a representation to decompose the homography matrix into 8 orthogonal flow bases. Hong *et al.* [16] utilized the GAN [36] model to enhance the feature similarity supervision. Additionally, some unsupervised methods, such as NeMAR [18], RFNet [37], and UMF-CMGR [19], utilize modality transfer networks to translate one modality into another, enabling unsupervised cross-modal motion estimation. The above unsupervised methods perform well on image pairs with small deformations, but may yield unsatisfactory results under large deformations and modality gaps.

3 Methodology

We propose InterNet, an interleaved modality transfer and self-supervised homography prediction network, designed to estimate the homography of cross-modal images in an unsupervised manner. As illustrated in Fig. 1 (a), InterNet consists of two learnable parts, a modality transfer module and a homography estimation module. The overall framework of InterNet can be divided into two phases: the self-supervised homography estimation phase and the modality transfer phase. In the self-supervised homography estimation phase, the homography estimation module learns to estimate the homography matrices between input images, while the weights of the modality transfer module are frozen. In the modality transfer phase, the modality transfer module is trained to narrow the modality gaps between the input cross-modal images. Here, the weights of the homography estimation module are partially frozen, leaving only the feature extractor trainable to ensure feature consistency. These two phases mutually enhance each other to achieve high-quality modality transfer and accurate cross-modal homography estimation during the training procedure. We further adopt a distillation training technique to enhance the network’s generalization ability and reduce the network parameters, as shown in Fig. 1 (c). The following sections introduce the details about the overall interleaved framework of our InterNet (Section 3.1), the supervision of our network (Section 3.2), and the distillation training process (Section 3.3).

3.1 Interleaved Framework

Self-supervised Homography Estimation Phase. Generating ground-truth homography of intra-modal images with simulated deformation is a common approach in previous works [7, 8, 11, 9]. However, cross-modal images are usually misaligned, making it impractical to obtain ground-truth cross-modal homography. Assuming there is a modality transfer module that can perfectly translate images from modality A to modality B. Ideally, when combined with the modality transfer module, the homography estimation module only requires to be trained with simulated intra-modal image pairs from modality B to achieve accurate cross-modal homography estimation. With the above consideration, we introduce a self-supervised homography estimation phase to leverage intra-modal supervision, enabling the homography estimation module to learn the direct knowledge of homography transformation in a self-supervised manner. We apply the simulated homography matrices to individually warp \mathbf{I}_A and \mathbf{I}_B , generating the intra-modal image pairs $(\mathbf{I}_A, \mathbf{I}'_A)$ and $(\mathbf{I}_B, \mathbf{I}'_B)$. The modality transfer module translates $(\mathbf{I}_A, \mathbf{I}'_A)$ into $(\mathbf{I}_{A,Trans}, \mathbf{I}'_{A,Trans})$. The practical implementations reveal that the pseudo image $\mathbf{I}_{A,Trans}$ after modality transfer still retains modality differences compared to the image \mathbf{I}_B . Under the inspiration of multitask learning [38], we simultaneously use

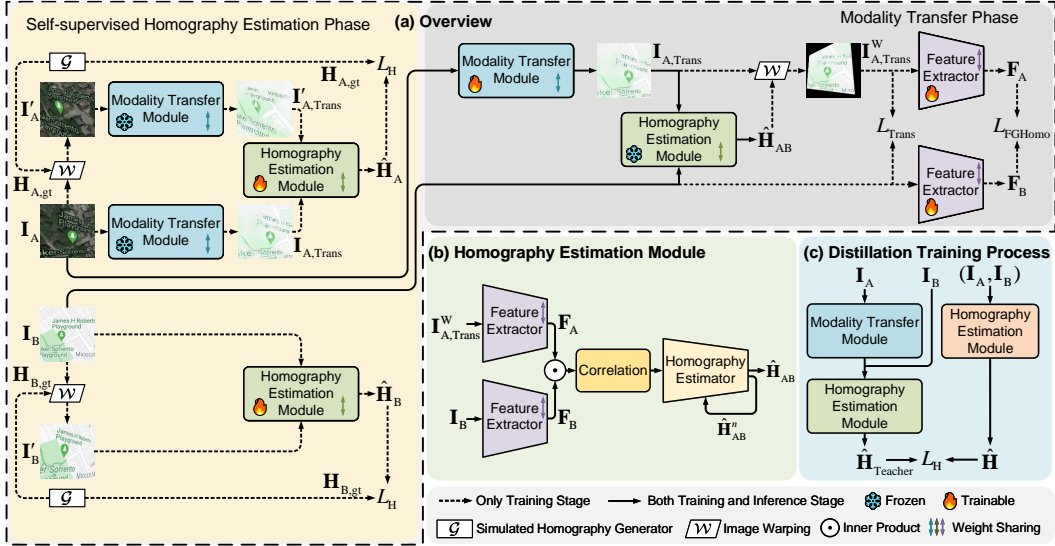


Figure 1: The schematic diagram of our interleaved modality transfer and self-supervised homography prediction network, named InterNet. (a) The overall schematic diagram of InterNet. (b) Detailed illustration of the homography estimation module. (c) The schematic diagram of distillation training process.

$(\mathbf{I}_B, \mathbf{I}'_B)$ and $(\mathbf{I}_{A,Trans}, \mathbf{I}'_{A,Trans})$ to train the homography estimation module. The knowledge of homography transformation between $\mathbf{I}_{A,Trans}$ and \mathbf{I}_B can be learned in an unsupervised way through a mechanism similar to the gradient aggregation of multitask learning [38, 39]. The training process in the self-supervised homography estimation phase can be expressed as

$$\arg \min_{\zeta} L_H(\mathcal{H}_{\zeta}(\mathbf{I}_{A,Trans}, \mathbf{I}'_{A,Trans}), \mathbf{H}_{A,gt}) + L_H(\mathcal{H}_{\zeta}(\mathbf{I}_B, \mathbf{I}'_B), \mathbf{H}_{B,gt}), \quad (1)$$

where \mathcal{H}_{ζ} denotes the homography estimation module with parameters ζ to be optimized, $\mathbf{H}_{A,gt}$ and $\mathbf{H}_{B,gt}$ are the simulated intra-modal homography matrices. We employ the correlation-based iterative homography estimation method IHN [11] as the basis of the homography estimation module, as shown in Fig. 1 (b). The feature extractor with shared weights extracts features of the input images, namely \mathbf{F}_A and \mathbf{F}_B . The homography estimator takes in the sampled correlation volume \mathbf{C} computed by \mathbf{F}_A and \mathbf{F}_B to iteratively estimates the homography. Notably, the correlation volume plays a crucial role in the iterative homography estimation. More consistent features can produce a more effective correlation volume, facilitating the homography estimator to achieve higher accuracy. The details about the homography estimation module are provided in Appendix A.2.

Modality Transfer Phase. The significant modality gaps in cross-modal images serve as one of the main challenges in cross-modal homography estimation. To address this challenge, we introduce a modality transfer phase in our framework. Specifically, we use a modality transfer module \mathcal{T} to translate \mathbf{I}_A into a pseudo modality B image $\mathbf{I}_{A,Trans}$. For the supervision of modality transfer, directly applying supervision on the misaligned $\mathbf{I}_{A,Trans}$ and \mathbf{I}_B is infeasible. Similarly, we can assume the existence of a homography estimation module capable of accurately estimating the homography $\mathbf{H}_{AB,gt}$ between $\mathbf{I}_{A,Trans}$ and \mathbf{I}_B . In this case, we can use $\mathbf{H}_{AB,gt}$ to obtain perfectly aligned cross-modal image pairs to supervise the modality transfer results. In real situations, the $\hat{\mathbf{H}}_{AB}$ predicted by the homography estimation module may have discrepancies compared to the ground-truth $\mathbf{H}_{AB,gt}$. Therefore, instead of using pixel-wise L_1 or L_2 loss, we apply perceptual loss [35] to capture high-level representations, ensuring better tolerance to alignment errors and achieving high-quality modality transfer results. The training process in the modality transfer phase can be formulated by

$$\arg \min_{\theta} L_{Trans}(\mathcal{W}(\mathcal{T}_{\theta}(\mathbf{I}_A), \hat{\mathbf{H}}_{AB}), \mathbf{I}_B), \quad (2)$$

where \mathcal{T}_{θ} denotes the modality transfer module with parameters θ to be optimized, \mathcal{W} denotes the image warping with the estimated homography. For simplicity, we use $\mathbf{I}_{A,Trans}^W$ to represent the $\mathcal{W}(\mathcal{T}_{\theta}(\mathbf{I}_A), \hat{\mathbf{H}}_{AB})$. The details about the modality transfer module are provided in Appendix A.1.

Interleaved Optimization. The core ingredient of InterNet is the interleaved optimization between the two phases in the framework. In the self-supervised homography estimation phase, the modality transfer module produces the image pair $(\mathbf{I}_{A, \text{Trans}}, \mathbf{I}'_{A, \text{Trans}})$ that exhibits similar modality characteristics with $(\mathbf{I}_B, \mathbf{I}'_B)$, facilitating the homography estimation module to learn the knowledge of cross-modal homography estimation. In the modality transfer phase, the homography estimation module predicts $\hat{\mathbf{H}}_{AB}$ to align $\mathbf{I}_{A, \text{Trans}}$ and \mathbf{I}_B , providing reliable supervision for the modality transfer module. The two phases are associated through $(\mathbf{I}_{A, \text{Trans}}, \mathbf{I}'_{A, \text{Trans}})$ and $\hat{\mathbf{H}}_{AB}$, refining the modality transfer and cross-modal homography estimation in an interleaved manner throughout the training procedure.

Fine-grained Homography Feature Loss. In practice, supervising the similarity between pseudo and real images after the modality transfer does not guarantee the consistency of features in homography estimation. This might impede the mutual promotion between the modality transfer and homography estimation modules, leading to sub-optimal solutions. To further boost the performance of InterNet, we propose a fine-grained homography feature (FGHomo) loss to provide additional supervision on the homography feature maps of $\mathbf{I}_{A, \text{Trans}}$ and \mathbf{I}_B . The modality transfer module and the feature extractor in the homography estimation module are trained together under the constraint of FGHomo loss, which can be formulated as

$$\arg \min_{\theta, \xi} L_{\text{FGHomo}}(\phi_{\xi}(\mathcal{W}(\mathcal{T}_{\theta}(\mathbf{I}_A))), \hat{\mathbf{H}}_{AB}, \phi_{\xi}(\mathbf{I}_B)), \quad (3)$$

where ϕ_{ξ} denotes the feature extractor with parameters ξ to be optimized. The FGHomo loss strengthens the connection between two phases of our interleaved framework, enhancing the feature consistency of $\mathbf{I}_{A, \text{Trans}}$ and \mathbf{I}_B . This further optimizes the correlation of the features, refining the cross-modal homography estimation accuracy. Finally, the entire training process in the modality transfer phase can be formulated as

$$\arg \min_{\theta, \xi} L_{\text{Trans}}(\mathcal{W}(\mathcal{T}_{\theta}(\mathbf{I}_A)), \hat{\mathbf{H}}_{AB}, \mathbf{I}_B) + L_{\text{FGHomo}}(\phi_{\xi}(\mathcal{W}(\mathcal{T}_{\theta}(\mathbf{I}_A))), \hat{\mathbf{H}}_{AB}, \phi_{\xi}(\mathbf{I}_B)). \quad (4)$$

Inference. As for the inference of InterNet, the modality transfer module first produces \mathbf{I}_A to $\mathbf{I}_{A, \text{Trans}}$, and then the homography estimation module estimates the homography $\hat{\mathbf{H}}_{AB}$ between $\mathbf{I}_{A, \text{Trans}}$ and \mathbf{I}_B . The implementation details are provided in Appendix B.

3.2 Network Supervision

Homography Estimation Loss. In the self-supervised homography estimation phase, we parameterize the homography by the four corner displacement vectors following [11, 8, 9]. The homography estimation module predicts the homography matrices iteratively with a total iteration of N . The homography estimation loss is computed as a weighted sum of the L_1 distance between the estimated and the ground-truth displacement vectors in all the iterations, which can be formulated by

$$L_H(\hat{\mathbf{D}}, \mathbf{D}_{\text{gt}}) = \sum_{n=0}^{N-1} \alpha^{(N-n-1)} \left\| \hat{\mathbf{D}}^n - \mathbf{D}_{\text{gt}} \right\|_1, \quad (5)$$

where $\hat{\mathbf{D}}^n$ denotes the estimated displacement in iteration n , \mathbf{D}_{gt} denotes the ground-truth displacement. α is a coefficient less than 1, ensuring the later estimations to have larger weights.

Modality Transfer Loss. In the modality transfer phase, we warp image $\mathbf{I}_{A, \text{Trans}}$ with the estimated $\hat{\mathbf{H}}_{AB}$ for the modality transfer supervision and apply perceptual loss [35] as the modality transfer loss, which is formulated as

$$L_{\text{Trans}}(\mathbf{I}_{A, \text{Trans}}^W, \mathbf{I}_B) = \sum_j \frac{1}{C_j H_j W_j} \left\| \psi_j(\mathbf{I}_{A, \text{Trans}}^W) - \psi_j(\mathbf{I}_B) \right\|_2^2, \quad (6)$$

where ψ_j is the j -th layer of the pre-trained VGG with a feature map of shape $C_j \times H_j \times W_j$.

Correlation-based FGHomo Loss. We formulate the proposed FGHomo loss using a correlation-based loss function to further enhance the mutual promotion of two phases in our interleaved framework, which can be expressed as

$$L_{\text{FGHomo}}(\mathbf{F}_A, \mathbf{F}_B) = - \sum_{i,j} \mathbf{F}_A(i, j)^{\top} \mathbf{F}_B(i, j), \quad (7)$$

where \mathbf{F}_A and \mathbf{F}_B denote the feature maps of $\mathbf{I}_{A, \text{Trans}}^W$ and \mathbf{I}_B . The FGHomo loss directly constrains the correlation of features to produce more effective correlation results as the input of homography estimator, thereby obtaining more accurate homography estimation results.

3.3 Distillation Training for Robust Estimation

For the proposed InterNet, the modality transfer module is specifically designed to learn the mapping function between two modalities present in the training data. Therefore, when applied to other data domains, it may produce unsatisfactory modality transfer results. This leads to a marked decrease in the accuracy of homography estimation, compromising generalization and robustness.

To cope with the above problem, we employ a distillation training technique under the inspiration of the unsupervised knowledge distillation frameworks in domain adaptive object detection [40, 41]. We utilize the InterNet as a teacher model to guide a student model that only retains the homography estimation module, named Distilled InterNet (InterNet-D). During the distillation training process, the homography $\hat{\mathbf{H}}_{\text{teacher}}$ predicted by the InterNet serves as a pseudo ground-truth to supervise the InterNet-D, as illustrated in Fig. 1 (c). The distillation training process can be formulated by

$$\arg \min_{\omega} L_H(\delta_{\omega}(\mathbf{I}_A, \mathbf{I}_B), \hat{\mathbf{H}}_{\text{teacher}}), \quad (8)$$

where δ_{ω} denotes the homography estimation module of the InterNet-D with the parameters ω to be optimized.

Compared with the original InterNet, InterNet-D no longer relies on the modality transfer module, which significantly reduces the number of parameters. The experiments in Section 4.2 and Section 4.4 also indicate that InterNet-D significantly improves the cross-domain generalization ability while maintaining comparable performance.

4 Experiments

4.1 Experimental Settings

Datasets. We evaluate InterNet on various datasets, including GoogleMap [10], DPDN [20], WHU-OPT-SAR [21], and Flash/no-flash [22] cross-modal datasets, RGB/NIR [23] cross-spectral datasets, and PDS-COCO [17] photometrically distorted datasets. To ensure a fair comparison, all evaluated methods are trained and tested using the same training and test splits within each dataset.

Baselines. We evaluate InterNet with traditional feature-based approaches including SIFT [26], ORB [28], unsupervised approaches including UDHN [13], biHomE [17], CA-UDHN [14], Base-Homo [15], UMF-CMGR [19], and supervised approaches including DHN [7], MHN [8], LocalTrans [9], IHN [11], RHWF [12]. For feature-based approaches, we choose RANSAC [31] as the outlier rejection algorithms. UMF-CMGR is an image fusion approach based on registration, and we use the registration part for comparison.

Metrics. Similar to many previous works [7, 10–12, 9], we randomly perturb the corner points of 128×128 images to make the deformed image, with a perturbation range set to $[-32, 32]$. We evaluate homography estimation accuracy using the mean average corner error (MACE) following [7, 10–12, 9]. A lower MACE indicates a higher accuracy.

4.2 Comparisons with Existing Methods

Quantitative Comparison. We compare the homography estimation results of our proposed InterNet and baselines. We report the overall results of InterNet and the compared approaches on all 6 datasets in Table 1. It is observed that our method outperforms all the compared traditional and unsupervised approaches by a significant margin. The prior traditional and unsupervised approaches can hardly handle the homography estimation under large modality gaps. In contrast, our method achieves much more satisfactory results. Moreover, even though trained without direct cross-modal supervision, InterNet outperforms supervised approaches such as DHN, MHN and LocalTrans. Specifically, InterNet owns 54.3% and 47.4% lower MACEs than MHN, and 61.8% and 85.8% lower MACEs than LocalTrans on the challenging GoogleMap and WHU-OPT-SAR datasets, respectively.

Table 1: Quantitative comparison between our InterNet and other approaches. NC denotes the training is not converged. The best results of unsupervised methods are **highlighted in bold**. GM denotes GoogleMap, WOS denotes WHU-OPT-SAR, FNF denotes Flash/no-flash, RN denotes RGB/NIR, and PDS denotes PDS-COCO.

Methods		GM	DPDN	WOS	FNF	RN	PDS
Traditional	SIFT [26]	24.53	25.14	24.82	18.29	21.33	5.95
	ORB [28]	24.52	24.86	24.90	20.22	22.67	12.36
Unsupervised	UDHN [13]	22.84	NC	NC	21.20	23.43	10.75
	CA-UDHN [14]	24.61	24.99	24.76	21.32	24.12	24.89
	biHomE [17]	NC	NC	NC	11.86	23.77	2.61
	BasesHomo [15]	24.49	27.33	26.72	25.12	24.41	25.18
	UMF-CMGR [19]	24.60	25.46	24.70	23.49	22.38	23.26
	InterNet (Ours)	1.23	1.12	2.94	1.08	1.66	0.28
	InterNet-D (Ours)	1.26	1.24	3.31	1.16	1.72	0.33
Supervised	DHN [7]	5.20	4.92	8.27	6.42	11.88	2.50
	MHN [8]	2.69	2.95	5.59	5.24	5.52	1.22
	LocalTrans [9]	3.22	1.79	20.68	1.52	1.72	0.79
	IHN [11]	0.92	1.17	1.67	0.80	1.63	0.21
	RHWF [12]	0.71	1.06	1.48	0.65	1.07	0.09

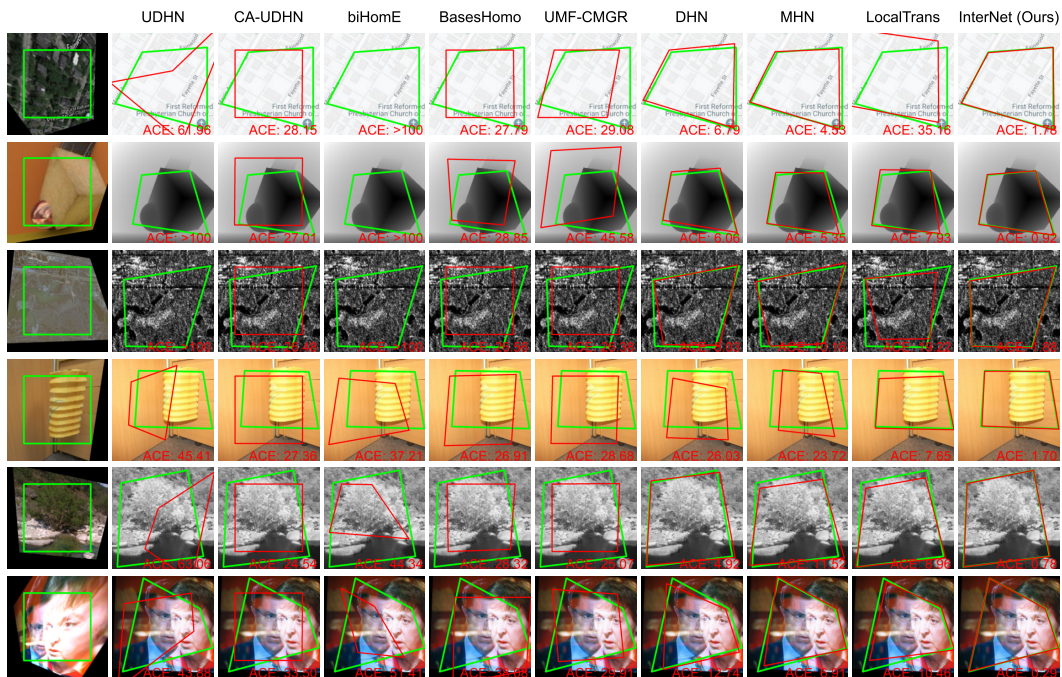


Figure 2: Qualitative homography estimation results on GoogleMap, DPDN, WHU-OPT-SAR, Flash/no-flash, RGB/NIR and PDS-COCO datasets. **Green** polygons denote the ground-truth homography deformation from I_A to I_B . **Red** polygons denote the estimated homography deformation using different approaches.

As mentioned in Section 3.1, we adopt the IHN architecture in the homography estimation module. We note that our method demonstrates better performance compared to the supervised IHN on DPDN. Intuitively, the strong contour correspondence in RGB and depth images on DPDN enables the modality transfer module to achieve high-quality results, while the FGHomo loss facilitates

the homography estimation module to extract more discriminative features, leading to a superior performance. We also conduct the distillation training on all datasets and present the results below InterNet in Table 1. We observe that the performance of InterNet-D is comparable to that of InterNet when supervised by the pseudo ground-truth.

Qualitative Comparison. We further illustrate the homography estimation results of some aforementioned methods in Fig. 2. It is observed that UDHN, biHomE, CA-UDHN, BasesHomo, and UMF-CMGR all struggle to find reasonable results, while DHN, MHN, and LocalTrans produces relatively more accurate homography estimations with direct supervision. Our InterNet achieves higher accuracy than DHN, MHN, and LocalTrans, which demonstrates the significant potential of our InterNet for real-world applications.

4.3 Ablation

The ablation analysis is conducted on the WHU-OPT-SAR test set, including two perspectives: the training strategy of the interleaved framework, and the modality transfer and fine-grained homography feature loss functions. We also evaluate the performance of different architectures in the modality transfer and homography estimation modules and report the results in Appendix C.

Training Strategy. We conduct an ablation study on the training strategy of our InterNet. As shown in Table 2, replacing intra-modal self-supervision with intensity-based cross-modal supervision lead to non-convergence due to the weak connection between intensity-based similarity metrics and the knowledge of homography transformations. For the self-supervision, using only real image pairs disrupts the module connection, preventing the network from converging. Meanwhile, using only pseudo image pairs after modality transfer enables the network to learn cross-modal homography estimation knowledge when the image pairs are gradually migrated to another modality, but the remaining modality differences still cause suboptimal performance. In contrast, supervising with both pseudo and real image pairs yields the optimal results.

In Table 2, we also note that the interleaved optimization framework is crucial for InterNet. Without interleaved optimization, jointly updating the weights of both modules leads to non-convergence. Conversely, interleaved training of the modality transfer and homography estimation modules decouples the optimization into simpler sub-problems, allowing each module to focus on its task, ensuring better convergence.

Loss Functions. To further investigate the effect of the modality transfer and fine-grained homography feature loss functions, we first train the network without the FGHomo loss and evaluate the performance of different types of modality transfer loss. The results in Table 3 indicate that the perceptual loss L_{pcp} outperforms L_1 and L_2 . Then we adopt L_{pcp} as the default modality transfer loss and add different types of FGHomo loss to analyze its impact. We report the results in the right part of Table 3. It is notable that though all different FGHomo loss types further boost the network’s performance, the correlation-based loss L_{corr} achieves superior performance compared to L_1 and L_2 . The correlation-based loss enhances the consistency of the two feature maps in the homography estimation module to produce a more effective correlation volume, further boosting the homography estimation accuracy.

Table 2: Ablation study on the self-supervised training strategy for the homography estimation module and the interleaved training strategy for the overall framework.

Experiment	MACE
intensity-based supervision	NC
self-supervision only on real	NC
self-supervision only on pseudo	5.93
self-supervision on both	2.94
w/o interleaved optimization	NC
interleaved optimization	2.94

Table 3: Ablation study on the loss functions. Trans denotes the modality transfer loss, FGHomo denotes the fine-grained homography feature loss.

Experiment	Loss Type	MACE
Trans	L_1	5.88
	L_2	6.23
	L_{pcp}	4.52
Trans+FGHomo	$L_{pcp} + L_1$	4.09
	$L_{pcp} + L_2$	3.27
	$L_{pcp} + L_{corr}$	2.94

Table 4: The cross-dataset evaluation results. The experimental results where over 50% of the homography predictions under an ACE of 5 on the test set are **highlighted in bold**. GM denotes GoogleMap, WOS denotes WHU-OPT-SAR, RN denotes RGB/NIR, FNF denotes Flash/no-flash, and PDS denotes PDS-COCO.

Train \ Test		GM	DPDN	WOS	FNF	RN	PDS
		GM	InterNet	98.3%	0.5%	0.4%	5.3%
	InterNet-D	98.4%	2.3%	1.4%	85.7%	72.4%	95.6%
DPDN	InterNet	1.5%	99.1%	0.1%	0.7%	1.6%	1.4%
	InterNet-D	68.0%	99.3%	0.5%	92.7%	77.6%	97.1%
WOS	InterNet	5.8%	0.3%	95.1%	2.9%	3.0%	3.1%
	InterNet-D	54.6%	1.6%	92.2%	80.3%	69.5%	93.6%
FNF	InterNet	8.5%	0.3%	0.2%	97.7%	87.7%	98.9%
	InterNet-D	3.3%	0.1%	0.1%	97.3%	83.1%	98.7%
RN	InterNet	49.5%	2.4%	1.8%	95.1%	94.1%	98.6%
	InterNet-D	49.0%	3.7%	4.8%	97.0%	94.0%	99.4%
PDS	InterNet	5.1%	0.4%	0.4%	99.1%	91.2%	99.7%
	InterNet-D	0.5%	0.1%	0.2%	98.7%	89.6%	99.6%

4.4 Cross-Dataset Generalization

We further conduct a cross-dataset evaluation of our InterNet and InterNet-D on the aforementioned datasets. The results are listed in Table 4. For each experiment, we report the percentage of homography predictions under an average corner error (ACE) of 5 on the test set, which reveals the ratio of reliable estimations.

We observe that both InterNet and InterNet-D perform well when trained and tested on the same dataset. However, InterNet shows poor generalization ability when trained on challenging datasets such as GoogleMap, DPDN, and WHU-OPT-SAR. This is attributed to the modality transfer module’s inadequate performance caused by significant modality differences across datasets. In contrast, InterNet-D trained on challenging datasets exhibits superior generalization ability. Through distillation training, InterNet-D excludes the modality transfer module and directly extracts consistent features from cross-modal image pairs. This enables InterNet-D to develop homography estimation capabilities on easier datasets including RGB/NIR, Flash/no-flash, and PDS-COCO after training on challenging datasets. We also note that InterNet and InterNet-D trained on the easier datasets demonstrate comparable performance in cross-dataset experiments.

The cross-dataset evaluation results indicate that InterNet-D effectively leverages the guidance of InterNet, achieving improved generalization and robustness while maintaining comparable homography estimation accuracy.

5 Conclusions

In this paper, we proposed a novel unsupervised cross-modal homography estimation framework, based on interleaved modality transfer and self-supervised homography prediction, named InterNet. Our InterNet introduces an interleaved optimization to narrow modality gaps and improve cross-modal homography estimation performance alternatively. We also design a fine-grained homography feature loss to further improve the connection between two modules and boost the estimation accuracy. Moreover, we employ a distillation training technique to reduce model parameters and improve cross-domain generalization ability. Experimental results show that our InterNet achieves SOTA performance on multiple challenging datasets among unsupervised approaches, and outperforms many supervised approaches.

References

- [1] Hunter Goforth and Simon Lucey. GPS-denied UAV localization using pre-existing satellite imagery. In *Proceedings of the IEEE International Conference on Robotics and Automation*, pages 2974–2980. IEEE, 2019.
- [2] Xiaolong Wang, Runsen Xu, Zhuofan Cui, Zeyu Wan, and Yu Zhang. Fine-grained cross-view geo-localization using a correlation-aware homography estimator. *Advances in Neural Information Processing Systems*, 36, 2023.
- [3] Iman Marivani, Evaggelia Tsiligianni, Bruno Cornelis, and Nikos Deligiannis. Designing CNNs for multimodal image restoration and fusion via unfolding the method of multipliers. *IEEE Transactions on Circuits and Systems for Video Technology*, 32(9):5830–5845, 2022.
- [4] Fayaz Ali Dharejo, Muhammad Zawish, Farah Deeba, Yuanchun Zhou, Kapal Dev, Sunder Ali Khowaja, and Nawab Muhammad Faseeh Qureshi. Multimodal-boost: Multimodal medical image super-resolution using multi-attention network with wavelet transform. *IEEE/ACM Transactions on Computational Biology and Bioinformatics*, 2022.
- [5] Yuan Zhou, Anand Rangarajan, and Paul D Gader. An integrated approach to registration and fusion of hyperspectral and multispectral images. *IEEE Transactions on Geoscience and Remote Sensing*, 58(5):3020–3033, 2019.
- [6] Jiacheng Ying, Hui-Liang Shen, and Si-Yuan Cao. Unaligned hyperspectral image fusion via registration and interpolation modeling. *IEEE Transactions on Geoscience and Remote Sensing*, 2021.
- [7] Daniel DeTone, Tomasz Malisiewicz, and Andrew Rabinovich. Deep image homography estimation. *arXiv preprint arXiv:1606.03798*, 2016.
- [8] Hoang Le, Feng Liu, Shu Zhang, and Aseem Agarwala. Deep homography estimation for dynamic scenes. In *Proceedings of the IEEE/CVF Conference on Computer Vision and Pattern Recognition*, pages 7652–7661, 2020.
- [9] Ruizhi Shao, Gaochang Wu, Yuemei Zhou, Ying Fu, Lu Fang, and Yebin Liu. LocalTrans: A multiscale local transformer network for cross-resolution homography estimation. In *Proceedings of the IEEE/CVF International Conference On Computer Vision*, pages 14890–14899, 2021.
- [10] Yiming Zhao, Xinming Huang, and Ziming Zhang. Deep lucas-kanade homography for multimodal image alignment. In *Proceedings of the IEEE/CVF Conference on Computer Vision and Pattern Recognition*, pages 15950–15959, 2021.
- [11] Si-Yuan Cao, Jianxin Hu, Zehua Sheng, and Hui-Liang Shen. Iterative deep homography estimation. In *Proceedings of the IEEE/CVF Conference on Computer Vision and Pattern Recognition*, pages 1879–1888, 2022.
- [12] Si-Yuan Cao, Runmin Zhang, Lun Luo, Beinan Yu, Zehua Sheng, Junwei Li, and Hui-Liang Shen. Recurrent homography estimation using homography-guided image warping and focus transformer. In *Proceedings of the IEEE/CVF Conference on Computer Vision and Pattern Recognition*, pages 9833–9842, 2023.
- [13] Ty Nguyen, Steven W Chen, Shreyas S Shivakumar, Camillo Jose Taylor, and Vijay Kumar. Unsupervised deep homography: A fast and robust homography estimation model. *IEEE Robotics and Automation Letters*, 3(3):2346–2353, 2018.
- [14] Jirong Zhang, Chuan Wang, Shuaicheng Liu, Lanpeng Jia, Nianjin Ye, Jue Wang, Ji Zhou, and Jian Sun. Content-aware unsupervised deep homography estimation. In *Proceedings of the European Conference on Computer Vision*, pages 653–669. Springer, 2020.
- [15] Nianjin Ye, Chuan Wang, Haoqiang Fan, and Shuaicheng Liu. Motion basis learning for unsupervised deep homography estimation with subspace projection. In *Proceedings of the IEEE/CVF International Conference On Computer Vision*, pages 13117–13125, 2021.

- [16] Mingbo Hong, Yuhang Lu, Nianjin Ye, Chunyu Lin, Qijun Zhao, and Shuaicheng Liu. Unsupervised homography estimation with coplanarity-aware GAN. In *Proceedings of the IEEE/CVF Conference on Computer Vision and Pattern Recognition*, pages 17663–17672, 2022.
- [17] Daniel Koguciuk, Elahe Arani, and Bahram Zonooz. Perceptual loss for robust unsupervised homography estimation. In *Proceedings of the IEEE/CVF Conference on Computer Vision and Pattern Recognition*, pages 4274–4283, 2021.
- [18] Moab Arar, Yiftach Ginger, Dov Danon, Amit H Bermano, and Daniel Cohen-Or. Unsupervised multi-modal image registration via geometry preserving image-to-image translation. In *Proceedings of the IEEE/CVF Conference on Computer Vision and Pattern Recognition*, pages 13410–13419, 2020.
- [19] Wang Di, Liu Jinyuan, Fan Xin, and Risheng Liu. Unsupervised misaligned infrared and visible image fusion via cross-modality image generation and registration. In *Proceedings of the International Joint Conference on Artificial Intelligence*, 2022.
- [20] Gernot Riegler, David Ferstl, Matthias R  ther, and Horst Bischof. A deep primal-dual network for guided depth super-resolution. In *British Machine Vision Conference*. The British Machine Vision Association, 2016.
- [21] Xue Li, Guo Zhang, Hao Cui, Shasha Hou, Shun Yao Wang, Xin Li, Yujia Chen, Zhijiang Li, and Li Zhang. MCANet: A joint semantic segmentation framework of optical and SAR images for land use classification. *International Journal of Applied Earth Observation and Geoinformation*, 106:102638, 2022.
- [22] Shengfeng He and Rynson WH Lau. Saliency detection with flash and no-flash image pairs. In *Proceedings of the European Conference on Computer Vision*, pages 110–124. Springer, 2014.
- [23] Matthew Brown and Sabine S  strunk. Multispectral SIFT for scene category recognition. In *Proceedings of the IEEE/CVF Conference on Computer Vision and Pattern Recognition*, pages 177–184. IEEE, 2011.
- [24] Simon Baker and Iain Matthews. Lucas-Kanade 20 years on: A unifying framework. *International Journal of Computer Vision*, 56:221–255, 2004.
- [25] Bruce D Lucas and Takeo Kanade. An iterative image registration technique with an application to stereo vision. In *Proceedings of the International Joint Conference on Artificial Intelligence*, volume 2, pages 674–679, 1981.
- [26] David G Lowe. Distinctive image features from scale-invariant keypoints. *International Journal of Computer Vision*, 60:91–110, 2004.
- [27] Herbert Bay, Tinne Tuytelaars, and Luc Van Gool. SURF: Speeded-up robust features. In *Proceedings of the European Conference on Computer Vision*, pages 404–417. Springer, 2006.
- [28] Ethan Rublee, Vincent Rabaud, Kurt Konolige, and Gary Bradski. ORB: An efficient alternative to SIFT or SURF. In *Proceedings of the IEEE/CVF International Conference On Computer Vision*, pages 2564–2571. IEEE, 2011.
- [29] Kwang Moo Yi, Eduard Trulls, Vincent Lepetit, and Pascal Fua. LIFT: Learned invariant feature transform. In *Proceedings of the European Conference on Computer Vision*, pages 467–483. Springer, 2016.
- [30] Jiaming Sun, Zehong Shen, Yuang Wang, Hujun Bao, and Xiaowei Zhou. LoFTR: Detector-free local feature matching with transformers. In *Proceedings of the IEEE/CVF Conference on Computer Vision and Pattern Recognition*, pages 8922–8931, 2021.
- [31] Martin A Fischler and Robert C Bolles. Random sample consensus: A paradigm for model fitting with applications to image analysis and automated cartography. *Communications of the ACM*, 24(6):381–395, 1981.
- [32] Daniel Barath, Jiri Matas, and Jana Noskova. MAGSAC: Marginalizing sample consensus. In *Proceedings of the IEEE/CVF Conference on Computer Vision and Pattern Recognition*, pages 10197–10205, 2019.

- [33] Paul W Holland and Roy E Welsch. Robust regression using iteratively reweighted least-squares. *Communications in Statistics-theory and Methods*, 6(9):813–827, 1977.
- [34] Che-Han Chang, Chun-Nan Chou, and Edward Y Chang. CLKN: Cascaded Lucas-Kanade networks for image alignment. In *Proceedings of the IEEE Conference on Computer Vision and Pattern Recognition*, pages 2213–2221, 2017.
- [35] Justin Johnson, Alexandre Alahi, and Li Fei-Fei. Perceptual losses for real-time style transfer and super-resolution. In *Proceedings of the European Conference on Computer Vision*, pages 694–711. Springer, 2016.
- [36] Ian Goodfellow, Jean Pouget-Abadie, Mehdi Mirza, Bing Xu, David Warde-Farley, Sherjil Ozair, Aaron Courville, and Yoshua Bengio. Generative adversarial nets. *Advances in Neural Information Processing Systems*, 27, 2014.
- [37] Han Xu, Jiayi Ma, Jiteng Yuan, Zhuliang Le, and Wei Liu. RFNet: Unsupervised network for mutually reinforcing multi-modal image registration and fusion. In *Proceedings of the IEEE/CVF Conference on Computer Vision and Pattern Recognition*, pages 19679–19688, 2022.
- [38] Rich Caruana. Multitask learning. *Machine Learning*, 28:41–75, 1997.
- [39] Carl Doersch and Andrew Zisserman. Multi-task self-supervised visual learning. In *Proceedings of the IEEE/CVF International Conference On Computer Vision*, pages 2051–2060, 2017.
- [40] Kuniaki Saito, Yoshitaka Ushiku, and Tatsuya Harada. Asymmetric tri-training for unsupervised domain adaptation. In *Proceedings of the International Conference on Machine Learning*, pages 2988–2997. PMLR, 2017.
- [41] Huayi Zhou, Fei Jiang, and Hongtao Lu. SSDA-YOLO: Semi-supervised domain adaptive yolo for cross-domain object detection. *Computer Vision and Image Understanding*, 229:103649, 2023.
- [42] Hu Cao, Yueyue Wang, Joy Chen, Dongsheng Jiang, Xiaopeng Zhang, Qi Tian, and Manning Wang. Swin-unet: Unet-like pure transformer for medical image segmentation. In *Proceedings of the European Conference on Computer Vision*, pages 205–218. Springer, 2022.
- [43] Ze Liu, Yutong Lin, Yue Cao, Han Hu, Yixuan Wei, Zheng Zhang, Stephen Lin, and Baining Guo. Swin transformer: Hierarchical vision transformer using shifted windows. In *Proceedings of the IEEE/CVF International Conference On Computer Vision*, pages 10012–10022, 2021.
- [44] Yousset I Abdel-Aziz, Hauck Michael Karara, and Michael Hauck. Direct linear transformation from comparator coordinates into object space coordinates in close-range photogrammetry. *Photogrammetric Engineering & Remote Sensing*, 81(2):103–107, 2015.
- [45] Ilya Loshchilov and Frank Hutter. Decoupled weight decay regularization. *arXiv preprint arXiv:1711.05101*, 2017.
- [46] Leslie N Smith and Nicholay Topin. Super-convergence: Very fast training of neural networks using large learning rates. In *Artificial Intelligence and Machine Learning for Multi-Domain Operations Applications*, volume 11006, pages 369–386. SPIE, 2019.

A Details of Modules

A.1 Details of Modality Transfer Module

Inspired by Swin-Unet [42], we adopt a transformer-based U-shaped generator as the modality transfer module, which consists of encoder, bottleneck, decoder and skip connections. We illustrate the architecture of the modality transfer module in Fig. 3. The input image \mathbf{I} is initially projected into feature space using a 3×3 convolutional layer. The encoder then processes the feature using 2 Swin Transformer blocks, a PixelShuffle layer, and an 1×1 convolutional layer to downsample the feature and expand its channel by $2 \times$. Correspondingly, the decoder upsamples the feature and reduces its channel by $2 \times$ using a PixelUnshuffle layer, an 1×1 convolutional layer, and 2 Swin Transformer blocks. Both two procedures are repeated four times in the modality transfer module. The bottleneck between the encoder and decoder is constructed with 6 Swin Transformer blocks to learn deep feature representations. The shallow and deep features are concatenated together via skip connections to complement the loss of spatial information caused by downsampling. At the end of the modality transfer module, an 1×1 convolutional layer projects the output feature into 3 channels, producing the modality transfer result $\mathbf{I}_{\text{Trans}}$.

The basic unit of the modality transfer module is Swin Transformer block [43], different from the standard multi-head self attention, Swin Transformer block first partitions the inputs into non-overlapping local windows, each window contains $M \times M$ patches. It computes the local attention for each window:

$$\text{Attention}(Q, K, V) = \text{SoftMax} \left(QK^T / \sqrt{d} \right) V, \quad (9)$$

where $Q, K, V \in \mathbb{R}^{M^2 \times d}$ denote the query, key and value matrices, M^2 is the number of patches in a window, d is the query/key dimension.

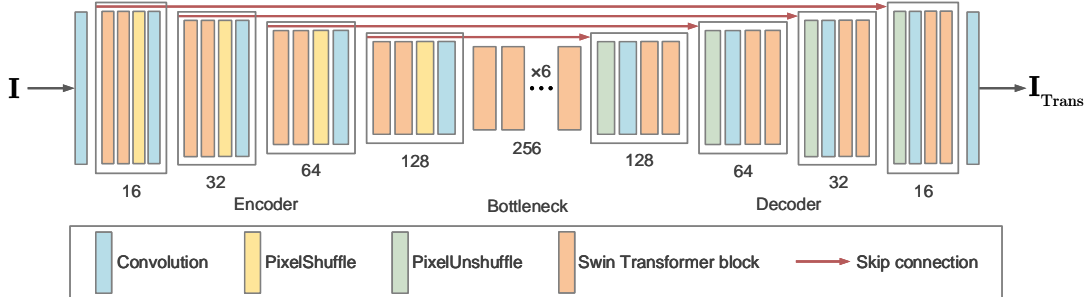


Figure 3: The detailed architecture of the modality transfer module.

A.2 Details of Homography Estimation Module

Feature Extraction. The architecture of the feature extractor is illustrated in Fig. 4 (a). The feature maps of two input images are produced by CNNs with shared weights. The input images are processed by a 7×7 convolutional layer and an instance normalization+ReLU layer to generate the feature maps. Then the features are further processed by two units. The first unit includes a max-pooling layer followed by 2 residual blocks with 64 channels. The second unit follows a similar pattern, but each residual block contains 96 channels. Each sequence performs a 2×2 downsampling, collectively producing the $1/4 \times 1/4$ resolution feature maps. Finally, the feature maps are expanded into 256 channels using an 1×1 convolutional layer.

Homography Estimator. The homography estimator is composed of multiple motion aggregation blocks, each consisting of a 3×3 convolutional layer, a group normalization+ReLU layer, and a max-pooling layer. As illustrated in Fig. 4 (b), the homography estimator takes in a correlation volume \mathbf{C} . With the motion aggregation blocks, the spatial resolution of the correlation volume diminishes to 2×2 . A convolutional layer of kernel size 1×1 then projects the output into a $2 \times 2 \times 2$ cube, producing the predicted residual offset vectors of the four corner points of the image.

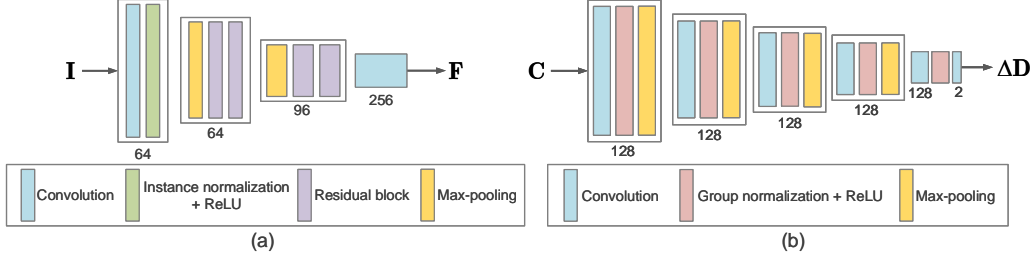


Figure 4: The detailed architectures of components in the homography estimation module. (a) The detailed architecture of the feature extractor. (b) The detailed architecture of the homography estimator.

Recurrent Homography Estimation. During the homography estimation, the feature extractor first extracts features of the input images. The correlation of the features is computed as

$$\mathbf{C}(\mathbf{F}_A, \mathbf{F}_B) \in \mathbb{R}^{H \times W \times H \times W}, \quad C_{ijkl} = \text{ReLU}(\mathbf{F}_A(i, j)^\top \mathbf{F}_B(k, l)), \quad (10)$$

where $\mathbf{F}_A, \mathbf{F}_B \in \mathbb{R}^{D \times H \times W}$ denote the feature maps of the input images. The estimation of homography is refined iteratively, the coordinate set \mathbf{X} in \mathbf{F}_A is projected by the present estimated homography $\hat{\mathbf{H}}^n$ to its corresponding coordinate set \mathbf{X}' in \mathbf{F}_B . In iteration n , the correlation volume \mathbf{C} is sampled by corresponding coordinate set \mathbf{X}^n with a local square grid of fixed search radius r , which can be formulated by

$$\mathbf{C}_S^n(\mathbf{x}) = \mathbf{C}(\mathbf{x}, \mathcal{N}(\mathbf{x}^n, r)), \quad (11)$$

where $\mathcal{N}(\mathbf{x}^n, r)$ denotes the local grid around \mathbf{x}^n with radius r . In iteration n , the homography estimator takes in the sampled correlation volume to predict the residual displacement vector $\Delta \hat{\mathbf{D}}^n$. In each iteration, $\Delta \hat{\mathbf{D}}^n$ is added to $\hat{\mathbf{D}}^{n-1}$, producing the updated displacement vector $\hat{\mathbf{D}}^n$. With $\hat{\mathbf{D}}^n$, the homography matrix $\hat{\mathbf{H}}^n$ can be obtained using the direct linear transform [44].

Homography Parameterization. Following previous methods, we parameterize the homography matrix using the displacement vectors of the four corner points as

$$\mathbf{A}\mathbf{h} = \mathbf{b}, \quad (12)$$

where \mathbf{b} is the coordinates of the warped four corner points, \mathbf{A} is composed of the warped four corner points and the original four corner points, \mathbf{h} is the vectorized \mathbf{H} . We define the four corner points in \mathbf{I}_A as (u_i, v_i) , in \mathbf{I}_B as (u'_i, v'_i) , where $i = 1, 2, 3, 4$. Then the predicted translation \mathbf{P} can be expressed as

$$\begin{aligned} u'_1 &= u_1 + \mathbf{P}(0, 0, 0), \\ v'_1 &= v_1 + \mathbf{P}(1, 0, 0), \\ u'_2 &= u_2 + \mathbf{P}(0, 0, 1), \\ v'_2 &= v_2 + \mathbf{P}(1, 0, 1), \\ u'_3 &= u_3 + \mathbf{P}(0, 1, 0), \\ v'_3 &= v_3 + \mathbf{P}(1, 1, 0), \\ u'_4 &= u_4 + \mathbf{P}(0, 1, 1), \\ v'_4 &= v_4 + \mathbf{P}(1, 1, 1). \end{aligned} \quad (13)$$

\mathbf{A} is formulated as

$$\mathbf{A} = \begin{bmatrix} u_1 & v_1 & 1 & 0 & 0 & 0 & -u_1 u'_1 & -v_1 u'_1 \\ 0 & 0 & 0 & u_1 & v_1 & 1 & -u_1 v'_1 & -v_1 v'_1 \\ u_2 & v_2 & 1 & 0 & 0 & 0 & -u_2 u'_2 & -v_2 u'_2 \\ 0 & 0 & 0 & u_2 & v_2 & 1 & -u_2 v'_2 & -v_2 v'_2 \\ u_3 & v_3 & 1 & 0 & 0 & 0 & -u_3 u'_3 & -v_3 u'_3 \\ 0 & 0 & 0 & u_3 & v_3 & 1 & -u_3 v'_3 & -v_3 v'_3 \\ u_4 & v_4 & 1 & 0 & 0 & 0 & -u_4 u'_4 & -v_4 u'_4 \\ 0 & 0 & 0 & u_4 & v_4 & 1 & -u_4 v'_4 & -v_4 v'_4 \end{bmatrix}, \quad (14)$$

and \mathbf{b} as

$$\mathbf{b} = [u'_1 \quad v'_1 \quad u'_2 \quad v'_2 \quad u'_3 \quad v'_3 \quad u'_4 \quad v'_4]^\top. \quad (15)$$

Finally, the vectorized \mathbf{H} is formulated as

$$\mathbf{h} = [\mathbf{H}_{11} \quad \mathbf{H}_{12} \quad \mathbf{H}_{13} \quad \mathbf{H}_{21} \quad \mathbf{H}_{22} \quad \mathbf{H}_{23} \quad \mathbf{H}_{31} \quad \mathbf{H}_{32}]^\top. \quad (16)$$

B Implementation Details

We implement our network using PyTorch, and train it with the AdamW [45] optimizer. The learning rate scheduler adopts OneCycleLR [46], with a maximum learning rate set to 3×10^{-4} . The training is conducted with a batch size of 16 for 120,000 iterations. We set the search radius $r = 4$ in the correlation sampling during the homography estimation and set $\alpha = 0.8$ in the homography estimation loss function. The total iteration N is set to 6. All the experiments are conducted on a single NVIDIA RTX4090 GPU.

C Additional Ablation on Module Architectures

We evaluate the performance of different architectures in the modality transfer module and homography estimation module. The results are listed in Table 5. It is evident that our InterNet struggles to deliver reliable results without the modality transfer module. For the modality transfer module, the transformer-based architecture demonstrates better performance compared to the CNN-based architecture with similar parameter counts.

In the right part of Table 5, we evaluate two correlation-based recurrent homography estimation architectures, IHN [11] and RHWF [12]. We note that RHWF does not outperform IHN in our interleaved framework, even though RHWF is the previous SOTA supervised approach. This result is reasonable because our interleaved framework is influenced by both modules simultaneously. When reaching convergence, it is difficult to enhance the overall performance simply through the optimization of a single module. As introduced the attention mechanism, RHWF incurs a higher computational cost compared to IHN. Thus we adopt IHN as the homography estimation module in our InterNet.

Table 5: Ablation study on the module architectures. The CNN-based and Transformer-based modality transfer architectures have similar parameter counts.

Module Architecture	MACE	Module Architecture	MACE
w/o modality transfer	26.20	IHN homography estimation	2.94
CNN-based modality transfer	8.72	RHWF homography estimation	3.08
Transformer-based modality transfer	2.94		

D Limitations

The interleaved training framework requires the modality transfer and homography estimation modules to be trained together, causing increased GPU memory requirements and longer training times.